Chapter: 4

Formulation and characterization of polyvinyl alcohol/chitosan composite nanofiber co-loaded with silver nanoparticle & luliconazole encapsulated poly lactic-co-glycolic acid nanoparticle for the treatment of *Candida* infected diabetic wounds

4 Formulation and characterization of polyvinyl alcohol/chitosan composite nanofiber co-loaded with silver nanoparticle & luliconazole encapsulated poly lactic-co-glycolic acid nanoparticle for treatment of *Candida* infected diabetic wounds

4.1 Plan of study

1. Fabrication of nanoparticle loaded nanofiber mat by electrospinning method
    a. Preparation of silver nanoparticles (AgNP) and luliconazole loaded PLGA nanoparticles (LZNP).
    b. Co-loading of nanoparticles within the polyvinyl alcohol and chitosan composite nanofiber matrix.
2. Morphological characterization of dual nanoparticle loaded PVA/CH nanofiber mat
    a. Transmission electron microscopy
    b. Scanning electron microscopy
    c. Atomic force microscopy
3. Solid State characterization
    a. Fourier transform infrared spectroscopy (FTIR)
    b. X-ray diffraction spectroscopy (XRD)
    c. Differential scanning calorimetry (DSC)
4. *In-vitro* characterization
    a. Surface pH study
    b. Contact angle study
    c. Water vapour transmission rate
    d. % Water uptake capacity
    e. Entrapment efficiency
    f. Content and weight uniformity
    g. *In-vitro* drug release & bio-imaging study
    h. Drug release kinetic modelling

i. Antifungal and antibiofilm activity

j. Cytocompatibility study

k. Hemocompatibility study

5. *In-vivo* characterization

a. Wound closure study

b. Histopathological examination

c. Laser doppler examination

4.2 Materials

Chitosan (medium molecular weight) and PVA (Polyvinyl alcohol, molecular weight ~125kD, 98-99.5% hydrolysis) were procured from Sigma Aldrich, India. TPGS NF grade (d-α-tocopheryl polyethylene glycol 1000 succinate) was obtained from ANTARES Health Product, INC. PLGA (Poly Lactic-Co-Glycolic Acid, Molecular Weight 7-17KD, Lactide and Glycolide (50:50)) and Luliconazole (LZ) were received as gift sample from Evonik Health care, Bangalore and Dr. Reddy Laboratories, Hyderabad, respectively. Silver Nitrate, Glutathione, methanol, acetonitrile, and dichloromethane were purchased from Sisco Research Laboratories Pvt. Ltd. HaCaT cell line was procured from NCCS Pune, India. DMEM, FBS, Trypsin-EDTA and penicillin-streptomycin solutions were purchased from Thermo Fisher Scientific, Mumbai, India. T-25 cell culture flask, 6 well cell culture plate and 96 well cell culture plate was purchased from Genetix Biotech Asia Pvt Ltd. All other materials were procured from certified vendors. Ultra-pure MiliQ water were used throughout experiment whenever needed.

4.3 Method

4.3.1 Preparation of nanoparticles

The synthesis of AgNP was conducted using previously reported method with minor modifications [217]. Briefly, a 50mL of aqueous solution containing ~85mg silver nitrate

(~10 mM) and ~77mg glutathione (5 mM) in a round bottom flask was placed into an oil bath, and maintained under continuous stirring and temperature of 90ºC, for a duration of 72 hours. The resultant product was lyophilised to obtain solid AgNPs, later used for microscopy and incorporation into nanofiber matrix.

The LZNPs were prepared using the solvent emulsification process [218]. Initially, a 5 mL of polymeric solution containing 10% w/v of PLGA, 1% w/v of LZ, and 4% w/v of TPGS was prepared using dichloromethane as solvent (organic phase). Then, 0.5% w/v & 0.1% w/v of polyvinyl alcohol (aqueous phase) were prepared. For nanoparticle preparation, 15 mL of 0.5% w/v PVA solution were transferred into 50 ml of glass tube (aqueous phase) maintained at 10°C temperature using an ice bath. Then, 2.5 ml of organic phase gradually added into the aqueous phase and subjected to probe sonication at an amplitude of 45% for 10 min. The resultant LZNPs were transferred to a beaker containing ~80 ml of 0.1% w/v aqueous PVA solution and stirred at 100rpm for overnight to allow the evaporation of organic solvent. Thereafter, the obtained LZNPs were washed with Ultra-pure MiliQ water and collected using high speed centrifugation at 15000rpm. The collected LZNPs were again redispersed in Ultra-pure MiliQ water and lyophilized to obtain dry powder, later used for microscopy and incorporation into nanofibers.

4.3.2 Preparation of nanoparticles loaded nanofibers

The nanoparticles loaded nanofiber was formulated using previously reported method [122]. Briefly, the solution-base for fabrication of nanofiber were prepared using PVA and chitosan (CH), and drugs were incorporated as per composition given in Table 4.1. Finally, solution-base was electrospun at a voltage of 10-15 KV, collecting plate at a distance of 10-15 cm, and flowrate of 0.5-1 ml/hr to obtain the nanofibers.

Table 4.1 Representation of the different proportion of drug and polymer used for fabrication of nanofibers.

S.No.	Formulation	PVA (10% w/v in water)	CH (3% w/v in 0.1% aq. acetic acid)	LZNP (% w/w)	AgNP (% w/w)
1	PVA NF	1	0	-	-
2	PVA-CH NF	0.7	0.3	-	-
3	PVA-CH-AgNP NF	0.7	0.3	-	5%
4	PVA-CH-LZNP NF	0.7	0.3	10%	-
5	PVA-CH-AgNP-LZNP NF	0.7	0.3	10%	5%

4.3.3 Morphological characterization

4.3.3.1 Transmission electron microscopy

The transmission electron microscope (FEI Tecnai G2 20 TWIN) was used to examine the size of prepared nanoparticles (AgNP and LZNP) and nanoparticles co-loaded nanofiber (PVA/CH-AgNP-LZNP NFs). For this, lyophilized nanoparticles were redispersed in double distilled water, diluted, and a single drop was placed onto a copper TEM grid with a mesh size of 300. For TEM analysis of nanoparticles loaded nanofibers, the nanofibers were directly electrospun over TEM grid. The grid were dried at room temperature and then observed under TEM [219].

4.3.3.2 Scanning electron microscopy

Scanning electron microscope (CARL ZEISS EVO - SEM MA15 / 18) was used to determine the morphology and diameter of PVA/CH NF, PVA/CH-AgNP NF, PVA/CH-LZNP NF, and PVA/CH-AgNP-LZNP NF. For this, nanofiber was placed over the sample holder, coated with gold using a spin coater and loaded into scanning electron microscope for analysis [220]. For scanning probe microscopy (SPM), PVA/CH-AgNP-LZNP NFs was electrospun over a glass slide and studied using scanning probe microscope (NT-MDT NTEGRA Prima)[221].

4.3.4 Solid state characterization

Fourier transform infrared spectroscopy (FTIR), X-ray diffraction spectroscopy (XRD) & differential scanning calorimetry (DSC) were employed for drug polymer interaction study, and determining encapsulation (NPs in NFs) and thermal behaviour of drug, polymers and nanofibers. The FTIR analysis were conducted for PLGA, LZ, LZNP, PVA, CH, PVA/CH NF, and PVA/CH-AgNP-LZNP NF within the spectral range of 4000 cm^{-1} to 400 cm^{-1} using the Bruker Alpha™ instrument. The XRD analysis was conducted within a 2 theta range of 7º-65º using the Rigaku Miniflex 600™ instrument. While DSC was done using a Shimadzu DSC-60 Plus instrument within a temperature range of 25 to 350°C. The heating rate was set at 10°C/min, and a nitrogen flow rate of 40 mL/min was used for purging.

4.3.5 *In-vitro* characterization

4.3.5.1 Surface pH and contact angle

The surface pH of all nanofiber mats (PVA NF, PVA/CH NF, PVA/CH-AgNP NF, PVA/CH-LZNP NF, and PVA/CH-AgNP-LZNP NF) were estimated by cutting and placing nanofiber aliquots (weight approximately 25mg) in a petri plate. Then surface nanofibers were moisten with PBS (pH 7.4 and the pH of nanofiber surface were recorded using pH metre probe [222]. For determining the wettability (wetting angle) of nanofibers, a sessile drop of water was added over the surface of nanofiber and time-dependent contact angle was noted using contact angle goniometer [223].

4.3.5.2 Water absorption capacity and vapour transmission rate

The water absorption capacity of all nanofibers were evaluated using previously reported procedure [224]. Briefly, a nanofiber pieces with an approximate size of 10 mg were cut from freshly prepared nanofiber samples and immersed into pH 7.4 phosphate-buffered saline (PBS) solution for 12 hours. After 12 hours, the nanofiber pieces were removed from the buffer solution, placed over a dried tissue paper to remove excess water and then

weighed. The percentage water uptake capacity of the nanofibers were determined using Equation 4.1. All reading was performed in triplicate and subsequently plotted against time.

$$\%\, Water\ uptake = \frac{Final\ weight\ of\ nanofiber - Initial\ weight\ of\ nanofiber}{Initial\ weight\ of\ nanofiber} * 100$$

Equation 4.1

Similarly, water vapour transmission rate of all nanofiber samples were calculated as per previous reported method with minor modifications [225,226]. Briefly, glass tubes with a mouth area of 1.86 cm^2 were taken and filled with PBS buffer. The mouths of glass tubes were covered with nanofiber samples and the sides of tube mouth were properly sealed with parafilm. All tubes were incubated at 37ºC for 12 hours and then weight of all tubes were measured. The water vapour transmission rate were calculated using Equation 4.2. All results were compared with water vapour transmission rate of open tube and plotted.

$$WVT = \frac{Initial\ weight\ of\ tube - Final\ weight\ of\ tube}{Area\ of\ tube * Time\ duration}$$

Equation 4.2

4.3.5.3 Entrapment efficiency and drug content uniformity

The entrapment efficiency of nanoparticles and nanofibers were determined using developed HPLC method [222]. For entrapment efficiency, 25mg of nanoparticle/ nanofiber samples was dissolved in 0.5 mL of trifluoroacetic acid. The dissolved sample was added dropwise into a test tube containing 10 mL of methanol, sonicated for 10 min and centrifuged at 10,000 rpm for 5 min. The supernatant was collected and injected into an HPLC system (Shimadzu HPLC with a C18 reverse phase column with a particle size of 5 μm) for determining drug concentration using methanol: 0.1% orthophosphoric acid

aqueous solution (70:30) as the mobile phase. Similarly, drug content uniformity was determined by estimating drug entrapment at different locations of same nanofiber sample.

4.3.5.4 *In-vitro* drug release and drug release kinetic modelling

The drug release study for LZNP and PVA/CH-AgNP-LZNP NF were conducted using dialysis membrane (SpectraProTM MWCO >1kD membrane) method [221]. Briefly, a definite weigh (~100mg) of sample was placed within dialysis membrane with 2 mL of PBS 7.4 pH buffer and both ends sealed. The membrane was then transferred to a 20 mL beaker containing 15 mL of PBS, maintained under continuous stirring using a magnetic stirrer. At predetermined intervals, 0.5 mL of sample was collected from outer compartment and examined using HPLC. To maintain the sink condition, 0.5 mL of fresh media was added into the outer compartment after each sampling. The drug release profile was fitted to various release models in order to predict the drug release mechanism. Similarly, the release of silver nanoparticle from PVA/CH-AgNP-LZNP NF was determined by reacting silver ions to 3,3′,5,5′-tetramethylbenzidin (TMB) and measuring the absorbance at 656 nm using UV spectrophotometer [227]. Briefly 200µL of 0.66mM of TMB solution (ethanol and sodium acetate buffer pH 4) were reacted with 100µL of collected samples for 15 min and % release were identified.

4.3.6 *In-vivo* bioimaging analysis

To visualise the payload release from nanofiber, 4µg/mL DID dye-encapsulated PLGA NP were prepared and loaded into PVA/CH nanofiber. The nanofibers were applied to a full thickness wound created on dorsal part of rat, and the fluorescent signals were recorded using in-vivo imaging system (Photon Imager, Optima Bio Space Lab) for 60 hours.

4.3.7 Antifungal & antibiofilm activity

The antifungal activity of PVA/CH NF, PVA/CH-AgNP NF, and PVA/CH-AgNP-LZNP NF were determined by agar plate method using CLSI guidelines against *C. albicans (ATCC 90028)*, *C. auris* (CDC-B11903), *C. tropicalis* (ATCC 750), *C. parapsilosis (ATCC 22019)*, *C. krusei (ATCC 6258)* [228]. In brief, 5 mL of each *Candida* species ($1.5*10^8$ cell/mL) were prepared in normal saline and dispersed using a cotton swab on previously prepared Mueller hinton agar plates. The petri plates were then bore with a standard punch and 2 mg of nanofiber sample were inserted in their respective positions. Each petri dishes were placed in an incubator set to 37°C for 24 hours. Then, zone of inhibition of each petri plate was measured using a vernier calliper and images were captured using a camera.

Similarly, antibiofilm activity of PVA/CH NF and PVA/CH-AgNP-LZNP NF were determined for 48 hours [229]. For this, 15 mg of aliquots were taken into 32 well microplate and inoculated with 0.5 McFarland ($\sim 10^6$ CFU/ml) with respective fungi species for 48 hours. After 48hours MTT assay were performed and % viability was determined. For SEM analysis, samples were collected after 48 hours of inoculation from the microplate and observed under scanning electron microscope as per earlier protocols [230].

4.3.8 Hemocompatibility study

The haemolytic activity of all fabricated nanofibers were determined by following reported method with minor modifications [184,231]. Briefly, 2 mL of blood was collected from healthy rats in heparinised vial and diluted with 2.5 mL of 7.4 pH PBS buffer. Prior to haemolysis study, nanofiber samples were equilibrated by dipping into the PBS for 30 min at 37°C. Then, nanofiber samples were transferred into diluted blood and incubated for 60 min. After incubation, the samples were centrifuged at 1000 rpm for 5 min and 200µL of supernatant from each group was transferred to 96 well plate for recording the

absorbance at 545 nm. For negative and positive control group, a mixture of blood in PBS and blood in distilled water (mixture of 4:5 provide 100% haemolysis) were taken, respectively. The percentage haemolysis was calculated using Equation 4.3.

$$\% \, Hemolysis = \frac{Test\ absorbance - Negative\ control\ absorbance}{Positive\ control\ absorbace - Negative\ control\ absorbance} * 100$$

Equation 4.3

4.3.9 *In-vitro* cytocompatibility Study

The *in-vitro* cytocompatibility study of the PVA/CH NF & PVA/CH-Ag-LTZ NF were performed as per literature with slight modifications [232]. The Human keratinocytes cells (HaCaT) were cultured in DMEM along with 10 % FBS and Penistrep™ antibiotic solution. The cells were grown in a CO_2 incubator maintained at 37℃ and 5% CO_2.

To determine the *in-vitro* cytocompatibility activity of PVA/CH NF and PVA/CH-AgNP-LZNP NF, 500 µg weigh nanofibers pieces was placed in 6-well cell culture plate prior to cell seeding. Then, cell suspension containing $3x10^4$ cells/mL was seeded in each well in three different plates. For MTT assay, the medium was removed and fresh MTT containing medium (300 µL) was added to each well at 24, 48 and 72 hours of incubation and incubated for 2 hrs at 37℃. After incubation the formed formazan crystals were dissolved by adding 300 µL of DMSO. For absorbance the solution was distributed in 96 well cell culture plate and absorbance was taken at 570nm. To validate the cytocompatibility morphologically, the cells were seeded following above protocol and treatment was given accordingly. After treatment, the images were captured at different time interval (24 hrs, 48 hrs and 72 hrs) under phase contrast microscope through EVOS FL imaging system at 100X magnification.

4.3.10 *In vivo* wound healing activity

The wound healing efficacy of PVA/CH NF, PVA/CH-AgNP NF, PVA/CH-LZNP NF and PVA/CH-AgNP-LZNP NF were evaluated in sprague-dawley rats as per institute animal ethical committee (IAEC) protocol with approval number **IIT(BHU)/IAEC/2023/II/005** [233]. The induction of diabetes in rats were first carried out using the streptozotocin and nicotinamide method [234,235]. Briefly, rats were i.p. injected 120 mg/kg of nicotinamide, followed by 55 mg/kg of streptozotocin after 15 min. After seven-days, fasting blood glucose levels in all animals were examined, and those with levels greater than 250mg/dL were chosen for further study. The selected animals were then distributed into five groups, namely untreated/gauze treated, PVA/CH NF, PVA/CH-AgNP NF, PVA/CH-LZNP NF and PVA/CH-AgNP-LZNP NF. Each group consisted of three animals (n=3). The dorsal surface of each animal was carefully clipped, and the hairs were removed using a depilatory cream to achieve a hair-free skin. Then, full-thickness wound of ~1.5cm diameter was created. Subsequently, each wound surface was infected with *Candida* and left untreated for 4 days. Then, at 4^{th} day each group was given the treatments. Thereafter, on 11^{th} & 18^{th} day of study (7th and 14^{th} day post treatment), granulated tissues of each treatment group were collected from wounds site for histological study and images of all wounds were captured using a DSLR camera.

4.3.11 Histopathological study

The histopathological examination of injury (wound site) prior and after treatment was conducted to determine the effect of designed nanofiber on wound healing. For this, granulation tissue area of wound was collected at predetermined intervals, rinsed with PBS, and then preserved in 5% formalin solution. The collected tissues were set in wax mould and a slice of about 10 µm was made by transverse section. The tissue sections were fixed

to a glass slide, stained with H&E stain and examined under optical microscope for histological changes [236].

4.3.12 Laser doppler study

The laser doppler analysis was conducted for comprehensive assessment of intricate dynamics of blood circulation as response to nanofibers applied at wound site. The technique was employed for investigating the blood flow across the surface of nanofibers at day 11 and 18 of study [237]. For this, rats were anaesthetize using a combination of ketamine and xylazine and blood flow assessment was done by positioning the wound site in the path of a laser Doppler camera, subsequently analysed using the advanced OSMOZONE™ software.

4.3.13 Statistical analysis

All results were statistically analysed using version 5.03 of graph pad prism. The results were shown with standard deviation (SD) in mean (*n = 3). For group comparison, ANOVA and Student's t - test were used at statistical significance of $p < 0.05$, $*p<0.01$, $**p<0.001$, and $***p<0.0001$.

4.4 Results

4.4.1 Preparation of PVA/CH-AGNP-LZNP NF

The glutathione-reduced AgNPs were circular to oval shape with a diameter ranging between 5–20 nm, as confirmed by TEM (**Figure 4.1**). The result was similar to previously reported data [238]. The size of LZNP was in range of 120±47 nm as observed in SEM. Similar results were observed in TEM and the particles were spherical in shape. TEM also confirmed the successful co-loading of AgNP and LZNP in PVA/CH-AgNP-LZNP NF. The AgNP were found to present in core of nanofiber as densely dispersed nanoparticles. While, LZNP were observed embedded in nanofibers (PVA/CH-AgNP-LZNP NF) as bulb

like structures (Figure 4.2). This could be due to larger size particles of LZNP distributed in nanofiber matrix.

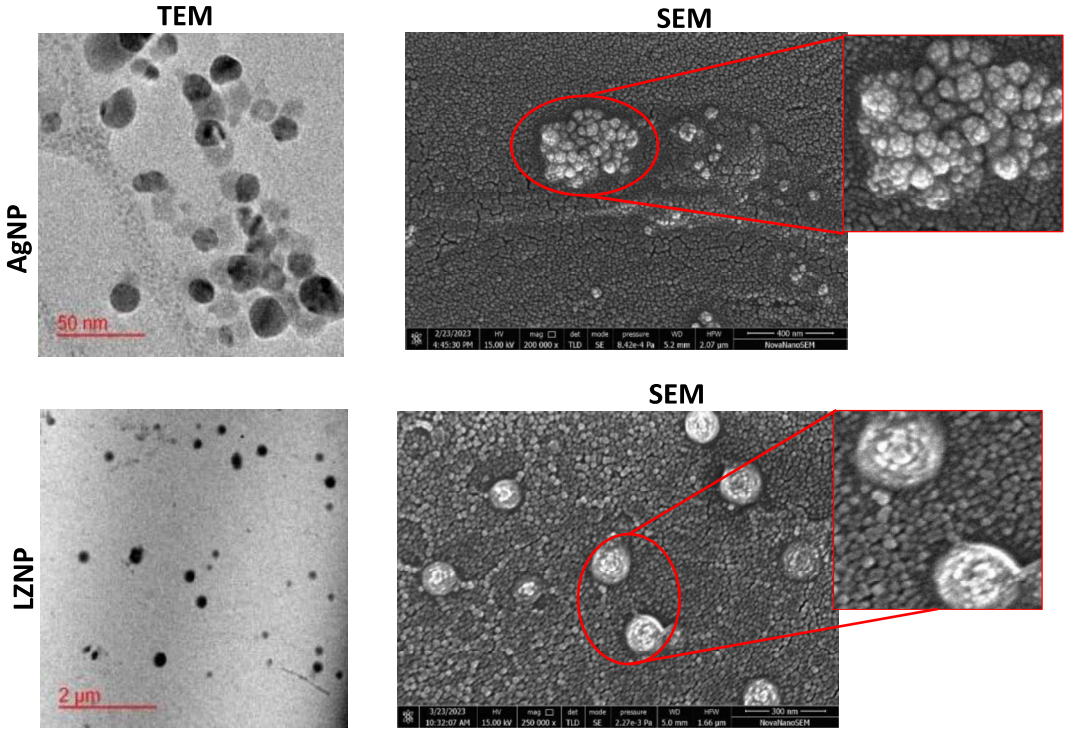

Figure 4.1 Transmission electron microscopy and scanning electron microscopy image of AgNP and LZNP.

4.4.2 Morphological characterization

The SEM analysis of PVA/CH NF revealed interconnected nanostructure with a size distribution of 190±43 nm (**Figure 4.3**). The incorporation of AgNP and LZNP in PVA/CH NF increased the average diameter of nanofiber to about 250±57 nm. LZNP particles in PVA/CH-AgNP-LZNP NF appeared as beads or bump like structures and the results were similar to TEM observations. Similar findings were observed in PVA/CH-AgNP NF and PVA-CH-LZNP NF with diameter of 217± 29 nm and 236± 31 nm, respectively. The AFM image of PVA/CH-AgNP-LZNP NF revealed a smooth surface with particles embedded widely over the surface of nanofiber (**Figure 4.2**).

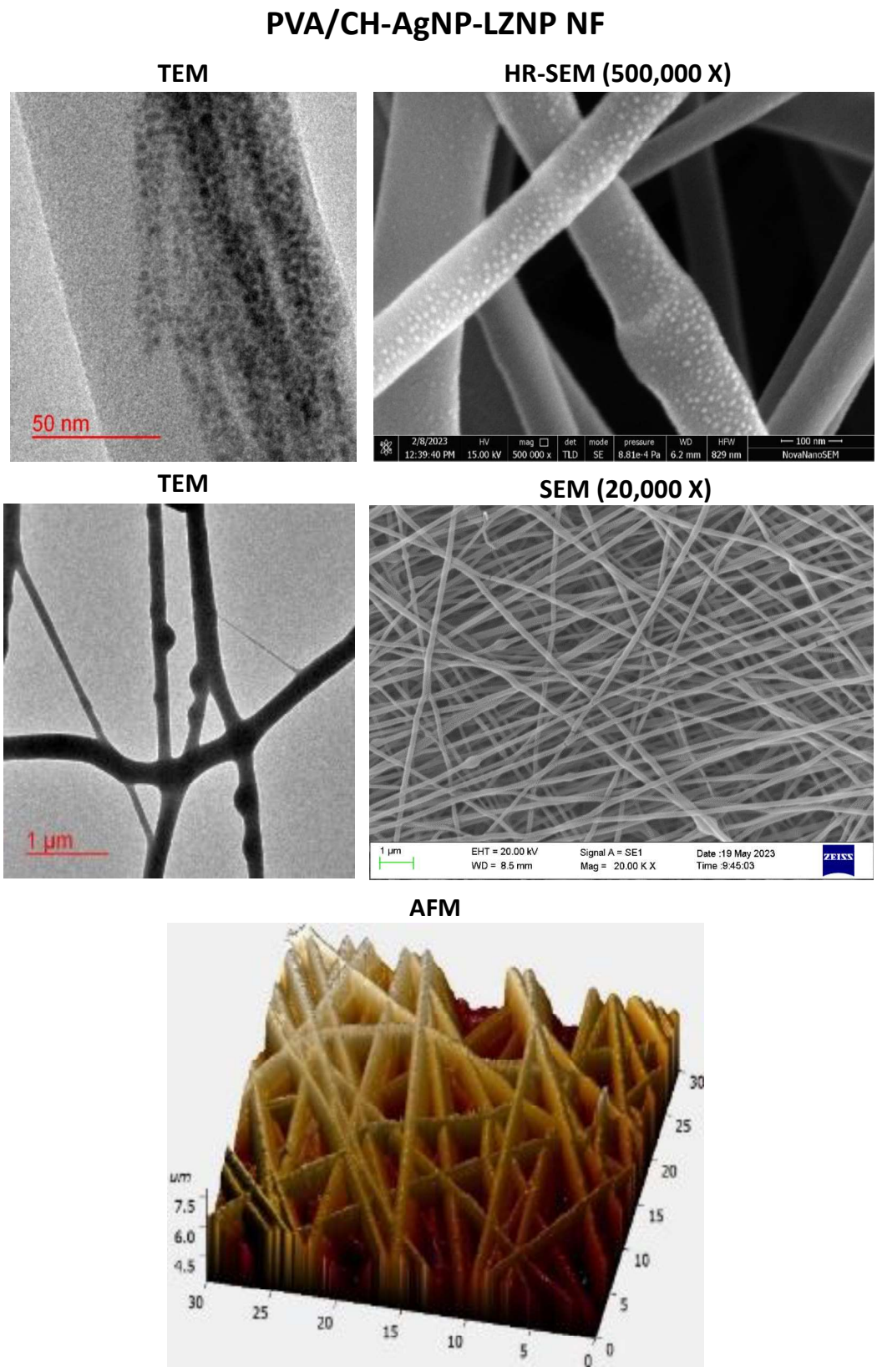

Figure 4.2 Transmission electron microscopy and scanning electron microscopy images of optimized PVA/CH-AgNP-LZNP nanofiber.

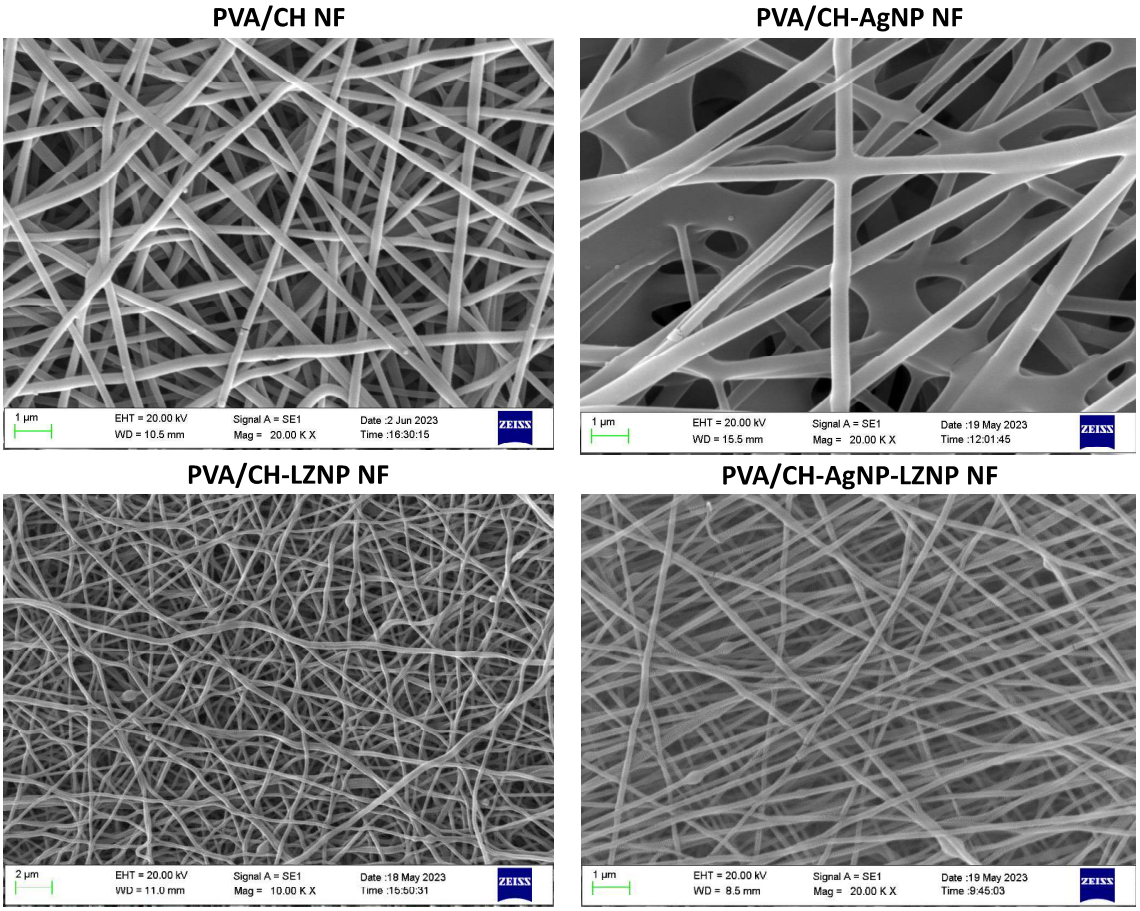

Figure 4.3 Scanning electron microscopy images of the PVA/CH NF, PVA/CH-AgNP NF, PVA/CH-LZNP NF and PVA/CH-AgNP-LZNP NF.

4.4.3 Solid-state characterization

4.4.3.1 Fourier transform Infrared spectroscopy (FTIR) study

The FTIR spectra (Figure 4.4) of PLGA showed peaks at 1758 cm^{-1} for C=O stretching vibration, 3414 cm^{-1} for O-H stretching and 2914 cm^{-1} for CH stretching [239,240]. LZ showed peaks at 3110 cm^{-1} for aromatic C-H stretching and 2920 cm^{-1} for aliphatic C-H stretching, at 1639 cm^{-1} an C=N stretching peaks and 1553 cm^{-1} C=C aromatic peaks also observed in spectra [199]. LZNP showed only major peaks of PLGA polymer (1752 cm^{-1} and 2910 cm^{-1} for C=O and C-H stretching, respectively) indicated successful encapsulation of LZ in nanoparticles and confirmed the compatibly of drug with polymer [218]. In addition, PVA showed transmission peaks at 3300cm^{-1} correspond to –OH

stretching, 2923 cm^{-1} for –CH_2 stretching vibrations , 1430 cm^{-1} for –C=O Stretching vibration, 1163 cm^{-1} for crystalline sequence peaks of PVA [241]. Chitosan showed characteristic peaks at 1645 cm^{-1} for C=O amide I stretching, 1322 cm^{-1} C-N stretching of amide IIIrd, and 1555 cm^{-1} for N-H bending of amide IInd. PVA/CH NF showed major peaks of PVA (3305 cm^{-1} for –OH stretching, 2922 cm^{-1} for –CH_2 stretching vibrations, and 1443 cm^{-1} for –C=O stretching vibration peaks) and chitosan (1592 cm^{-1} for amine group). Whereas, PVA/CH-AgNP-LZNP NF followed similar trend of nanoparticles, showing peaks of polymer used for fabrication of nanofibers. The results showed high compatibility with no new covalent bond formation and suggested proper encapsulation of nanoparticles in nanofiber [236].

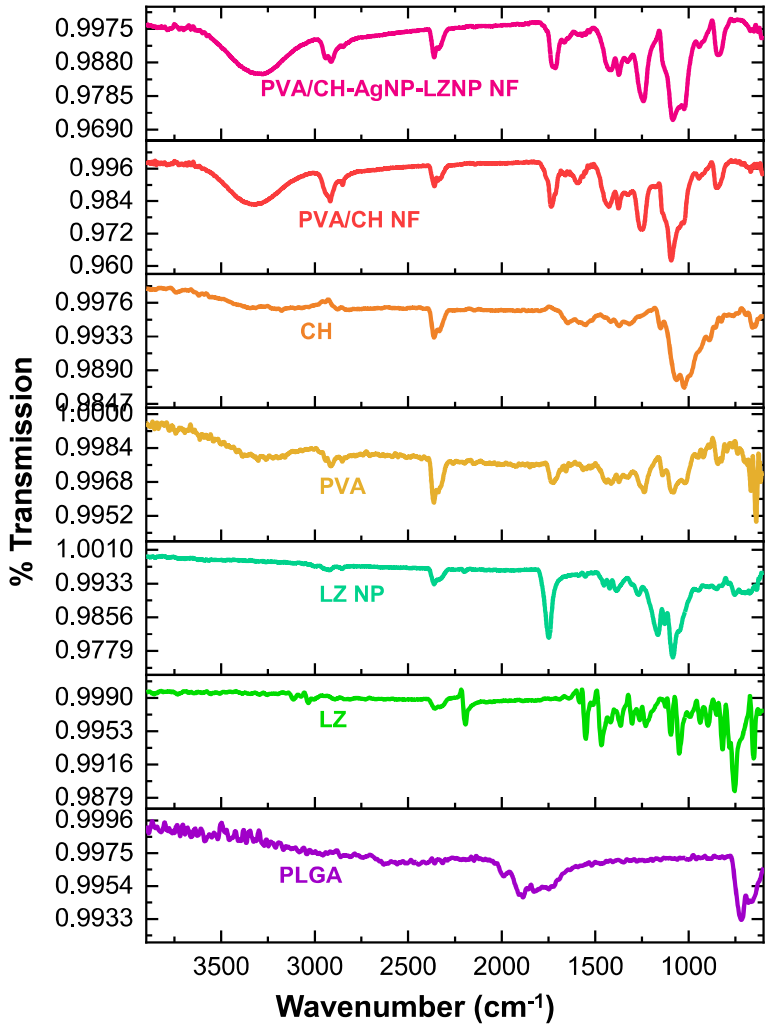

Figure 4.4 FT-IR spectra of drug, polymer and prepared nanofiber.

4.4.3.2 X-ray diffraction (XRD) study

XRD spectra (Figure 4.5) of PLGA showed a broad peak at about 20.4 º, showing amorphous nature of PLGA [218,242]. LZ showed multiple sharp crystalline peaks at 13.66 º, 16.34 º, 21.38 º, 23.34 º & 25.72 º. LZNP showed peaks similar to LZ however the intensity was reduced, probably due to encapsulation of drug in nanoparticles [199,242]. PVA showed major peaks at 19.860º and 22.84º, due to its semi-crystalline nature [243]. Chitosan had broader peaks at 20.3º and 10.3º due to its amorphous nature [244]. PVA/CH NF exhibited a high intensity peak at 24.28º corresponding to merge peak of PVA and chitosan. AgNP showed two characteristics peaks at 38.19 º and 46.18 º [245]. Whereas,

PVA/CH-AgNP-LZNP NF showed high intensity peak corresponding to PVA/CH NF and LZNP along with very small intensity peaks of AgNP, suggesting entrapment of nanoparticles in nanofiber matrix [246].

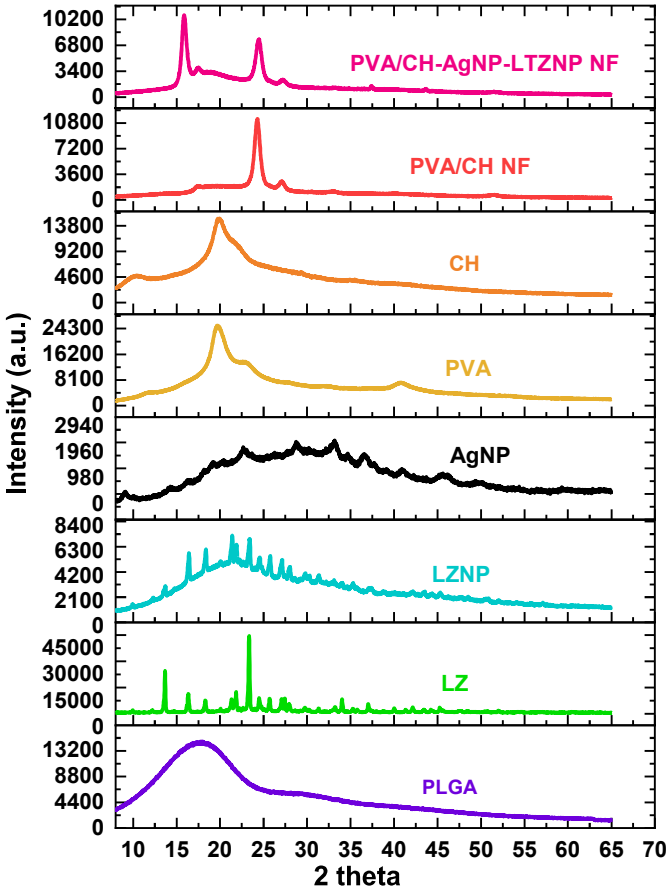

Figure 4.5 XRD spectra of drug (luliconazole), polymer and prepared nanofiber.

4.4.3.3 Differential scanning calorimetry (DSC) study

The DSC thermogram (Figure 4.6) of PLGA showed a glass transition dip at 52.24ºC and decomposition peak at 302.1ºC [247]. LZ showed a sharp endothermic peak at 151ºC corresponding to melting of crystalline LZ [199]. The absence of endothermic peak of LZ in LZNP could be due to encapsulation of drug in PLGA nanoparticles resulting in conversion of crystalline drug to amorphous state[199]. PVA showed an endothermic peak at 191ºC corresponding to its melting point, followed by broad peak at 302.14 ºC that could be due to the decomposition of PVA at higher temperature [248]. Chitosan exhibited two

endothermic peaks at 75°C and about 300°C. The first peak might be due to water loss and the second peak at 300°C due to the decomposition of amine units and glycosidic bond cleavage [249].

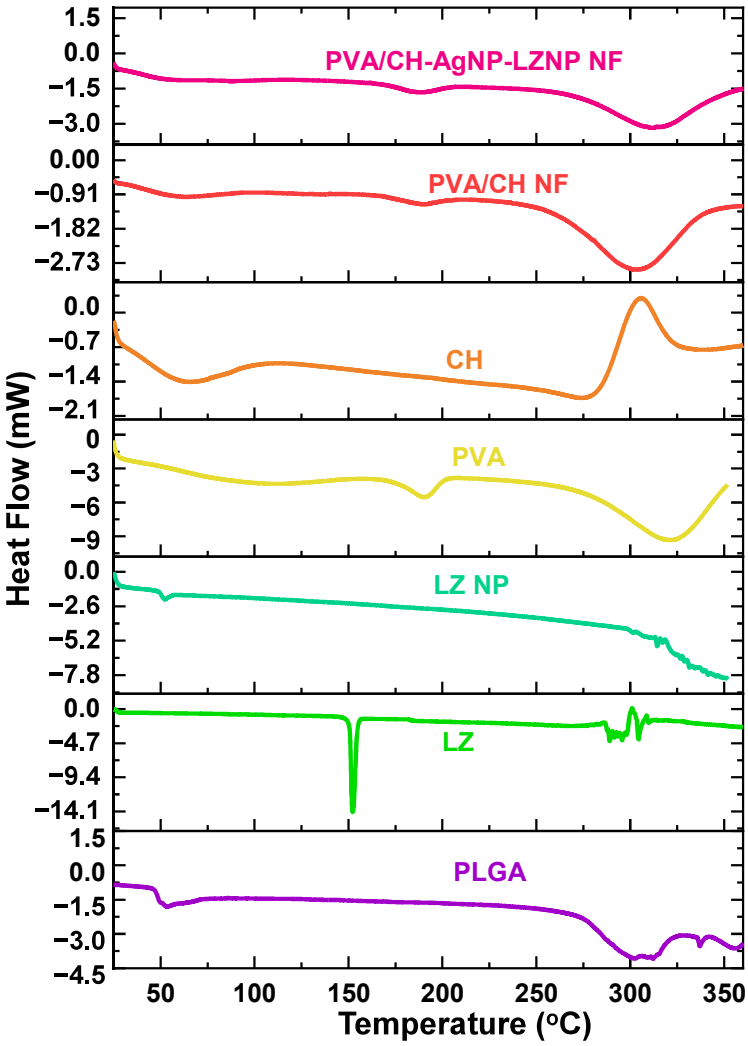

Figure 4.6 DSC thermogram of drug, polymer and prepared nanofiber.

PVA/CH NF and PVA/CH-AgNP-LZNP NF followed similar trend with only endothermic peak corresponding to polymer. The results were in agreement to FTIR and XRD and the absence of endothermic peak of drug confirmed encapsulation of nanoparticle in nanofiber matrix.

4.4.4 *In-vitro* characterization results

4.4.4.1 Contact angle and Surface pH

To confirm the wettability of prepared nanofibers, water contact angle of PVA NF, PVA/CH NF, PVA/CH-AgNP NF, PVA/CH-LZNP NF and PVA/CH-AgNP-LZNP NF was successfully determined that showed contact angle (°) of 38.7±3.9, 51.2±4.7, 54.9±4.8, 57.4±3.7 and 57.6±4.5, respectively at 70 sec (**Figure 4.7**). The time dependent water contact angle study was also conducted for PVA/CH-AgNP-LZNP NF that showed linear trend where contact angle (°) decreased from 84±3.1 to 56±4.2 (**Figure 4.7 A**). The study suggested that nanofiber had good wettability for application at target site. However, addition of chitosan in nanofibers resulted in significant increase (p value <0.05) in contact angle compared to only PVA NF. This could be due to low solubility of chitosan in neutral aqueous media. Additionally, the addition of nanoparticles (AgNP and LZNP) slightly increased the contact angle of nanofibers (PVA/CH-AgNP NF and PVA/CH-LZNP NF) probably due PLGA hydrophobicity. The surface pH study was conducted to determine the acceptability of nanofibers for topical application at desired site. Prepared nanofibers exhibited pH of 5.8 to 6.8 (Figure 4.7 D), which was within the limit for the topical formulations [250]. Although acetic acid was used for preparation of nanofiber base, still the pH of prepared nanofiber was within the desired range probably due to lower amount of solvent (0.1% aqueous acetic acid) used during nanofiber fabrication that have volatized while electrospinning at high voltage and storage in vacuum desiccator for overnight.

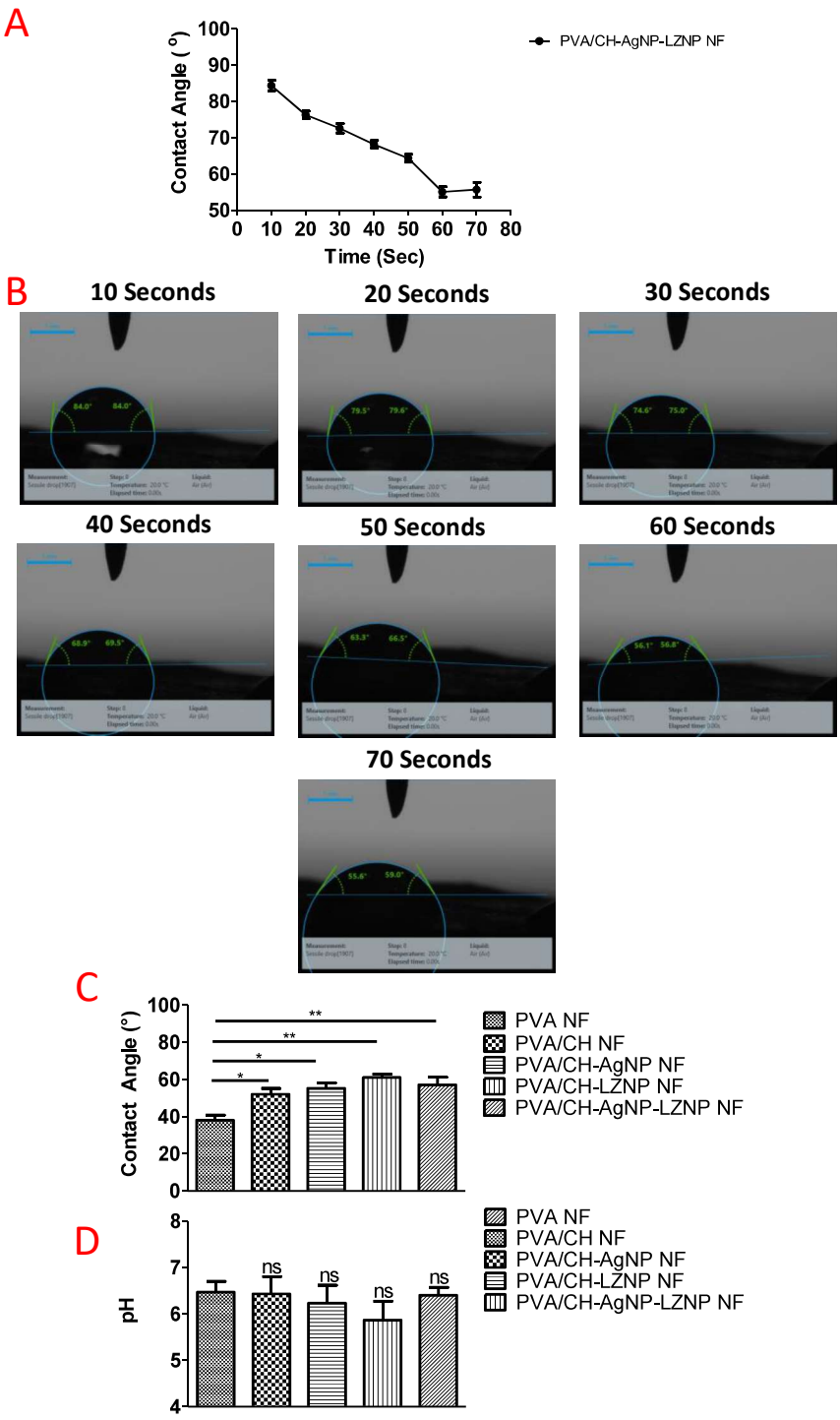

Figure 4.7 (A) Graphical representation of the PVA/CH-AgNP-LZNP NF water contact angle with respect to time (sec); (B) Contact angle of PVA/CH-AgNP-LZNP NF at different time points (sec); (C) Bar diagram for water contact angle image of PVA NF, PVA/CH NF, PVA/CH-AgNP NF, PVA/CH-LZNP NF and PVA/CH-AgNP-LZNP NF. (D) Surface pH of PVA NF, PVA/CH NF, PVA/CH-AgNP NF, PVA/CH-LZNP NF and PVA/CH-AgNP-LZNP NF nanofibers (In all graphs vertical bars represent standard

deviation (n=3), 'ns' represent non significant difference, * represent p value <0.05, and ** represent p value <0.01).

4.4.4.2 Water absorption capacity and water vapour transmission rate (WVTR)

Water absorption capacity of fabricated nanofibers were assessed to check the ability of nanofibers in absorbing wound exudate, an important characteristic of an ideal wound dressing materials. PVA NF demonstrated (Figure 4.8 A) water uptake of about 76±7.24%, while PVA/CH NF showed a two-fold increase in water uptake (135.35±4.90%) that could be due to incorporated chitosan responsible for high water absorption. The incorporation of AgNP and LZNP in nanofiber showed the water uptake capacity of 119±6.77%, 112.49±5.83%, and 107.12±7.84% for PVA/CH-AgNP NF, PVA/CH-LZNP NF and PVA/CH-AgNP-LZNP NF, respectively. This minor difference in water uptake capacity from PVA/CH nanofiber could be due to hydrophobic nature of PLGA nanoparticles.

Another important characteristic of wound dressing is maintenance of moisture around wound beds. Generally, moist wounds heal at a higher rate by two-fold compared to dry wounds. Therefore, WVTR of nanofibers plays key role in retaining wound moisture. The results showed a significant difference (p value <0.05) between WVTR of nanofibers and open tubes (Figure 4.8 B). The nanofibers exhibited WVTR of 6–18 mg/cm^2/hr, whereas open tube had WVT of ~38 mg/cm^2/hr. The results suggested higher capability of nanofibers in maintaining moist environment around wound area by reducing WVT by two-fold. The reduced transmission might be due to interconnected network of the nanofibers.

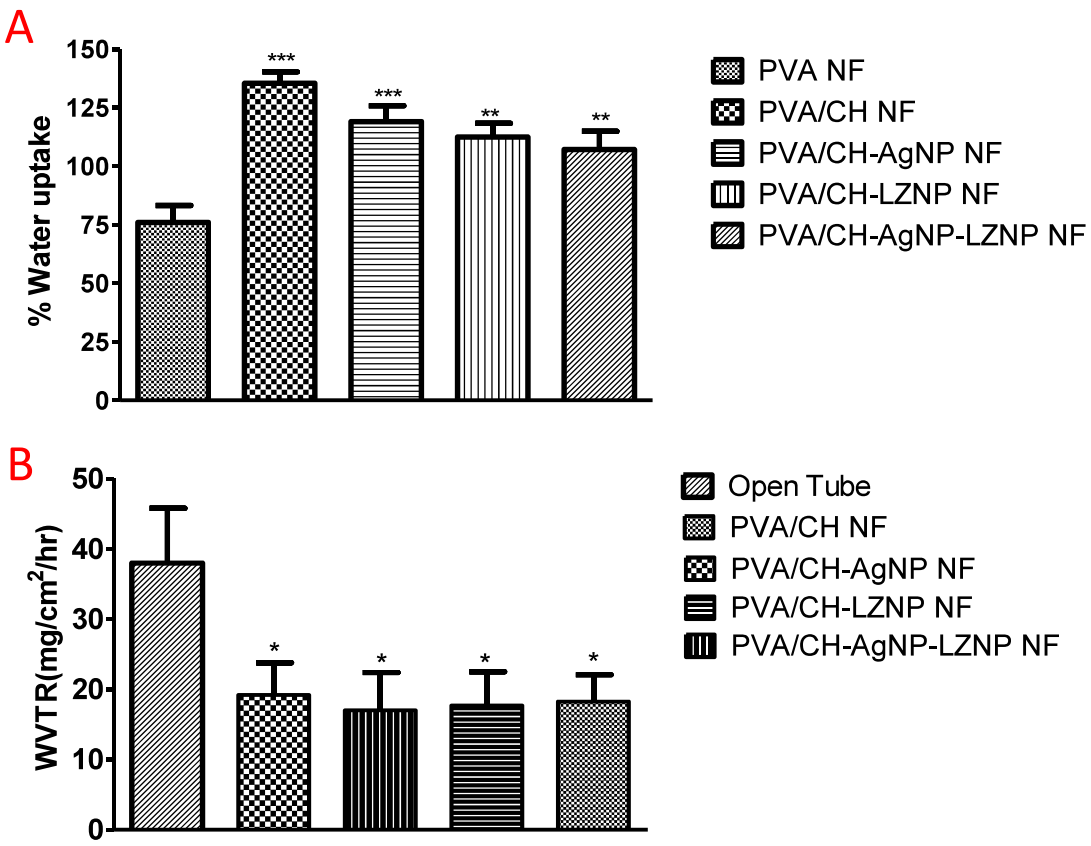

Figure 4.8 Bar graphs representing % water uptake capacity (A) & water vapour transmission rate (B) of PVA NF, PVA/CH NF, PVA/CH-AgNP NF, PVA/CH-LZNP NF and PVA/CH-AgNP-LZNP NF (In both graph vertical bars represent standard deviation (n=3), * represent p value <0.05, and ** represent p value <0.01 and *** represent p value < 0.001).

4.4.4.3 Entrapment efficiency and drug content uniformity

AgNP and LZNP showed an entrapment efficiency of 56.7±3.64% and 79.7±4.2% (Table 4.2). The entrapment efficiency of LZ in PVA/CH-LZNP NF and PVA/CH-AgNP-LZNP NF were 75.6±2.2% and 70.8±1.7%, respectively. Whereas, AgNP encapsulation in PVA/CH-AgNP NF and PVA/CH-AgNP-LZNP NF were 63.4±7.8 and 57.5±6.4%, respectively. Furthermore, drug content uniformity and weight variations results of all nanofibers showed a standard deviation < 5% that suggested highly uniform distribution of nanoparticles in nanofibers.

Table 4.2 Entrapment efficiency and average diameter of prepared nanoparticles and nanofiber mats

S.No.	Formulation	Average Diameter (nm)[#]	Entrapment Efficiency (%)*
1.	PVA/CH NF	190± 43 nm	-
2.	PVA/CH-AgNP NF	217± 29 nm	**63.4±2.8**
3.	PVA/CH-LZNP NF	236± 31 nm	**75.6±2.2**
4.	PVA/CH-AgNP-LZNP NF	250±57 nm	**57.5±4.4 for Ag+ & 70.8±1.7 for LZ**
5.	AgNP	5-20 nm	**56.7±3.64**
6.	LZNP	120±47 nm	**79.7±4.2**

mean±S.D (*n=3 & [#]n=150)

4.4.4.4 Drug release study

The drug release profile of LZ from of LZNP and PVA/CH-AgNP-LZNP NF were evaluated in PBS 7.4 buffer (Figure 4.10). The release of LZ was slower from PVA/CH-AgNP-LZNP NF compared to LZNP. LZNP showed an initial release of 19.45±3.3% for 90 min, followed by control release of LZ of about 67.1±4.1% in 144 hours. The LZNP incorporation into PVA/CH NF reduced the burst release 10.99±4.809% and provided about 51.18±3.75% LZ release in 144 hours. Additionally, release rate modelling showed an highest r^2 value of 0.9982 for LZNP and 0.9962 for PVA/CH-AgNP-LZNP NF fitting to Korrsemeyer Peppas model (Figure 4.9). The n value of 0.354 and 0.270 suggested release of LZ following non-fickian diffusion in supercase I (n value <0.45), suggesting release through erosion and swelling control diffusion. Further, release of silver ions from PVA/CH-AgNP-LZNP NF showed zero order release of silver ions for ~96 hours.

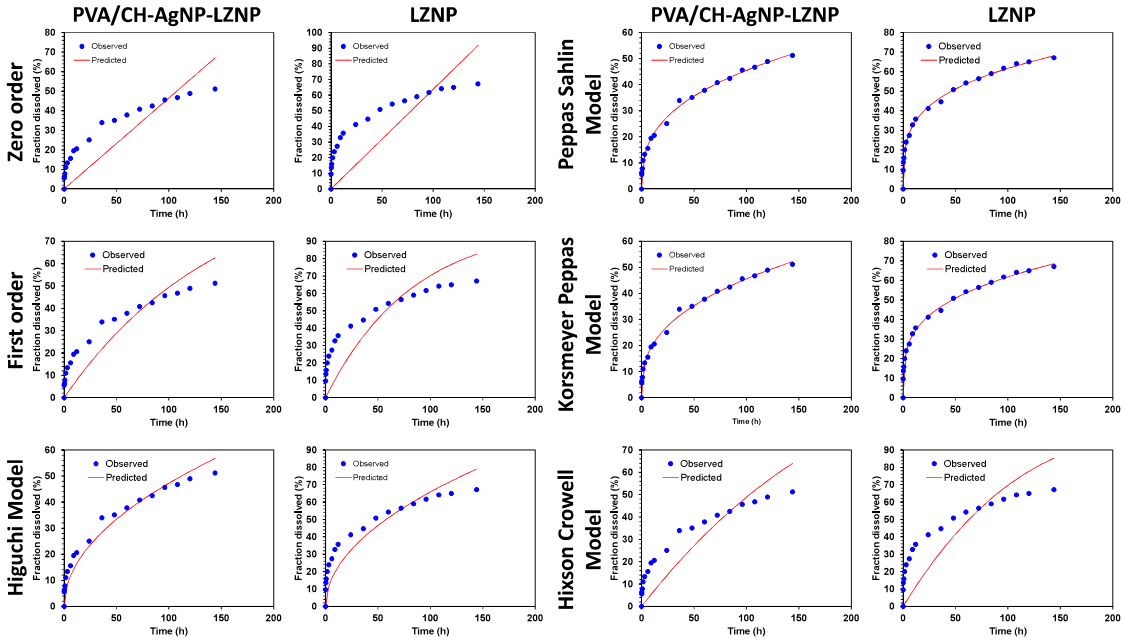

Figure 4.9 Drug release kinetic modelling of luliconazole from LZNP and PVA/CH-AgNP-LZNP NF formulation

4.4.5 *In-vivo* bio-imaging analysis

In-vivo imaging studies determined the release of encapsulated dye from nanofiber as a function of fluorescence count (**Figure 4.10 C**). The DID loaded nanofiber applied over the wound at 2 hours showed a fluorescence count of 3.38 x 10^6 that further increased gradually to a maximum count of 9.27 x 10^6 at 24 hours (**Figure 4.10** B). Thereafter, fluorescence count reduced following a downward trend, showing a florescence intensity of 3.61x10^6 at 60 hours. The trend was similar to drug release from nanofibers.

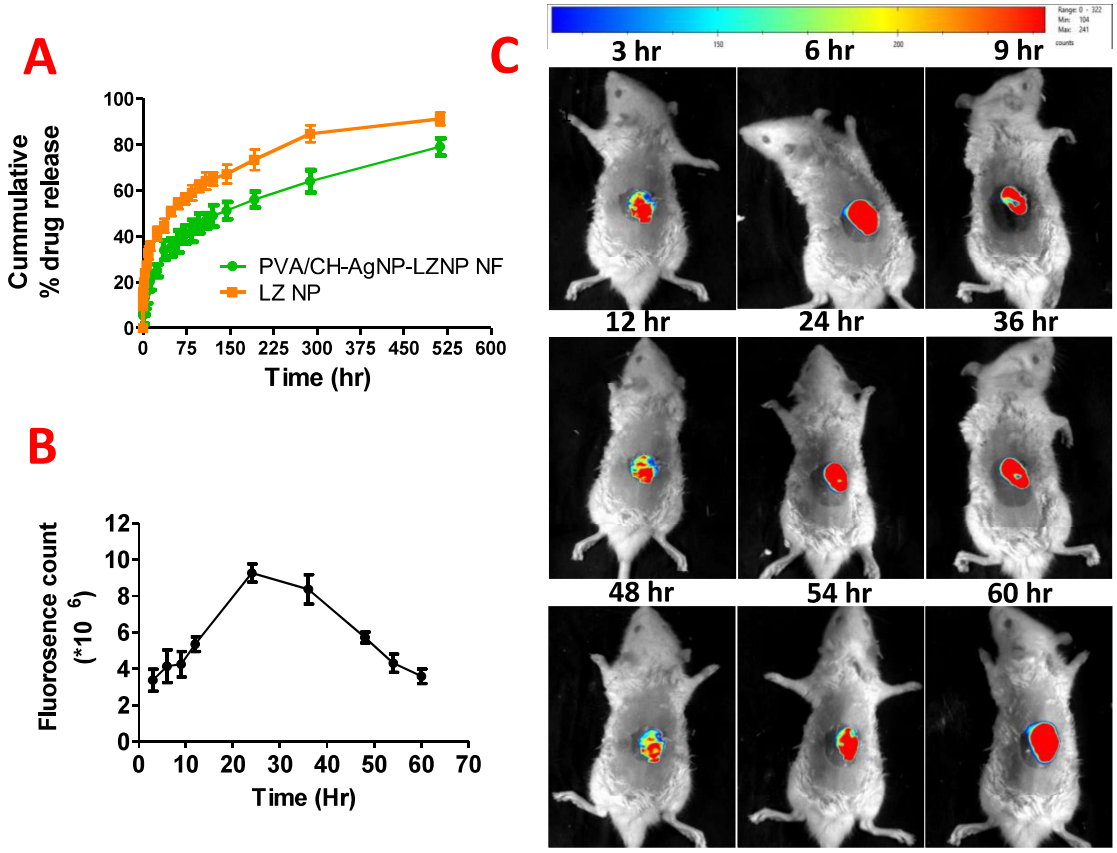

Figure 4.10 (A) *In-vitro* drug release of LZ from LZNP and PVA/CH-AgNP-LZNP NF; (B) Graphical representation of fluorescence count vs time (hr) response of DID-dye; and (C) *In-vivo* imaging study showing the release of encapsulated DID dye from nanofiber at wound site (In all figures vertical bar represent standard deviation (n=3)).

4.4.6 Antifungal and antibiofilm activity

The antifungal study of PVA/CH NF, PVA/CH-AgNP NF and PVA/CH-AgNP-LZNP NF were conducted successfully. PVA/CH NF had not shown any zone of inhibition (ZOI). In contrast, as shown in Figure 4.11**,** PVA/CH-AgNP NF and PVA/CH-AgNP-LZNP NF showed strong antifungal activity against various strains of *Candida*. The antifungal activity of PVA/CH-AgNP NF and PVA/CH-AgNP-LZNP NF showed zone of inhibition of 1.1±0.30mm & 17.48±0.82mm for *C. albicans*, 2.55±0.29mm & 14.7±1.15mm for *C. auris*, 8.985±1.110mm & 23.930±3.177mm for *C. tropicalis*, 8.901±3.776mm &

10.150±4.234mm for *C. parapsilosis*, and 17.802±1.08mm & 31.045±2.5mm for *C. krusei (ATCC 22019),* respectively.

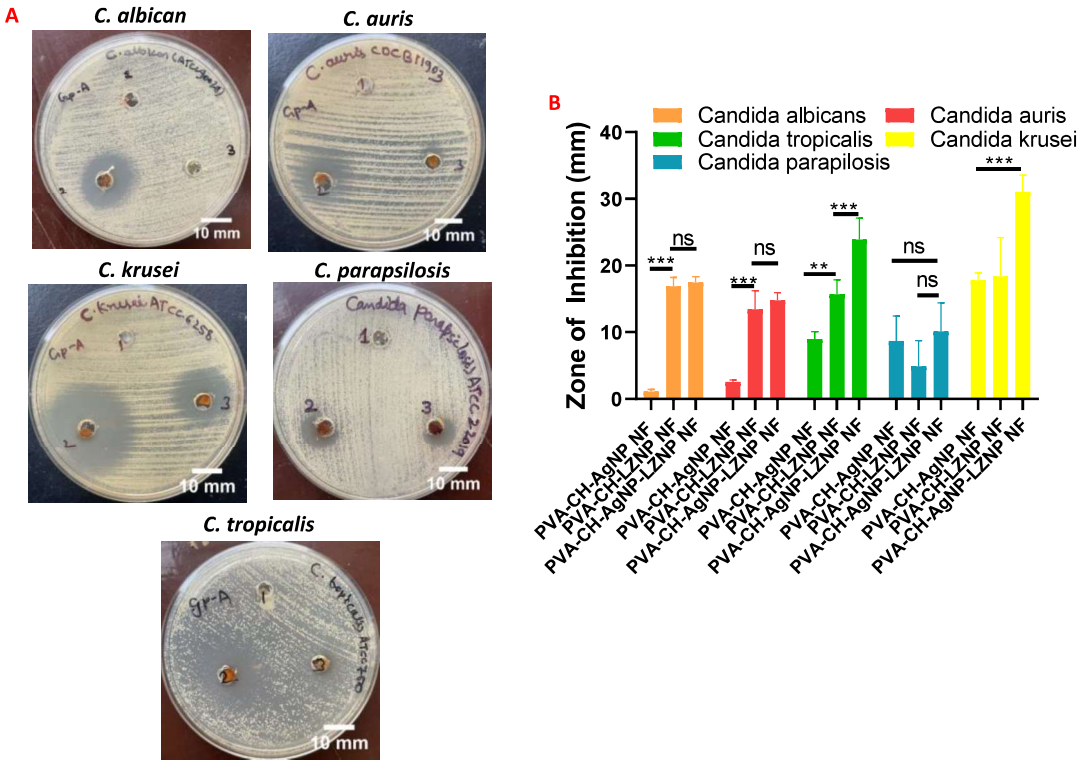

Figure 4.11 (A) Inhibition zone images of PVA/CH NF (1), PVA/CH-AgNP-LZNP NF (2) & PVA/CH-AgNP NF (3) showing antifungal activity against *C.albicans*, *C.auris, C.krusei*, *C.parapsilosis*, *C.tropicalis*; (B) Graphical representation of zone of inhibition (mm) values of PVA/CH-AgNP, PVA/CH-LZNP and PVA/CH-AgNP-LZNP NF (In graph vertical bars represent standard deviation (n=3), 'ns' represent non-significant, ** represent p value < 0.01 and *** represent p value < 0.001).

The antibiofilm activity of Control, PVA/CH NF and PVA/CH-AgNP-LZNP NF (Figure 4.12 A) confirm the potential of LZNP and AgNP loaded nanofibers in eradicating the fungal biofilm. Result showed 82.5±4.64% biofilm for *C.albicans* on treatment with PVA/CH NF probably due to chitosan. However, antibiofilm activity was not enough to irradicate the fungal strain to a larger extent. In contrast, PVA/CH-AgNP-LZNP NF showed only 15.33±7.44% biofilm. Similar results were observed for *C. tropicalis*, where PVA/CH NF showed 78.918±2.414% biofilm whereas PVA/CH-AgNP-LZNP NF showed only 11.140±7.215% biofilm**.** The results suggested that PVA/CH-AgNP-LZNP NF was

effective in eradicating *C. albicans* and *C. tropicalis* biofilm formation. The results were further confirmed by SEM (**Figure 4.12 B**), showing high effectiveness of PVA/CH-AgNP-LZNP NF in reducing *C. albicans* and *C. tropicalis* growth, as compared to PVA/CH NF.

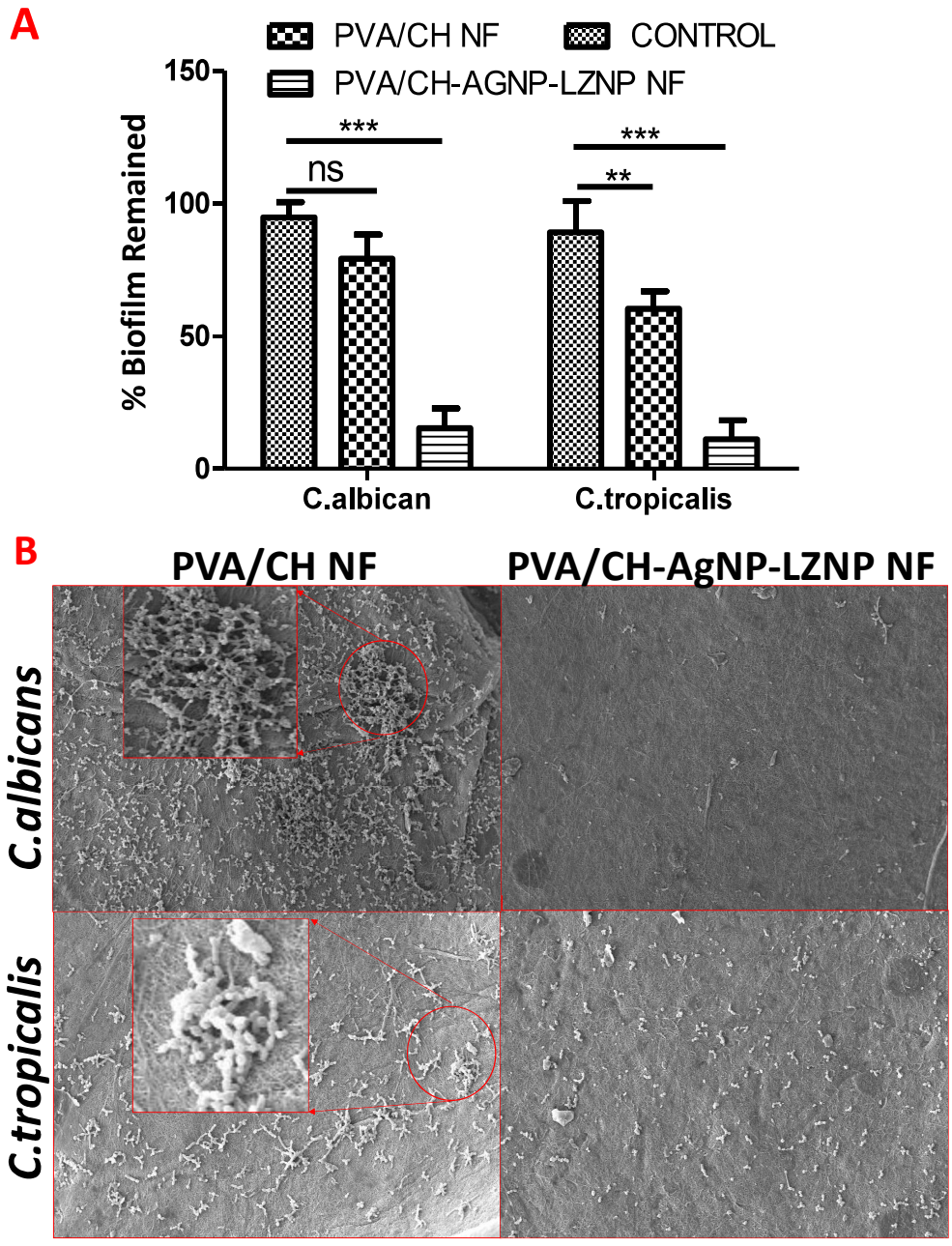

Figure 4.12 (A) Bar graph of MTT assay showing antibiofilm activity of control, PVA/CH NF and PVA/CH-AgNP-LZNP NF against *C.albicans* and *C.tropicalis*; (B) SEM images (500X) showing *C.albicans* and *C.tropicalis* after PVA/CH NF and

PVA/CH-AgNP-LZNP NF treatment (In graph vertical bars represent standard deviation (n=3), 'ns' represent non significant, ** represent p value < 0.01 and *** represent p value < 0.001).

4.4.7 Hemocompatibility study

All biomaterials that come into contact with blood must be hemocompatible and any adverse effect on blood components could be a sign of incompatibility. The hemocompatibility study showed 2.985±2.041% % of haemolysis for PVA/CH NF, 2.275±2.057% for PVA/CH-AgNP NF, 2.44±1.015% for PVA/CH-LZNP NF, and 3.49±1.485% for PVA/CH-AgNP-LZNP NF. The difference was significant (p value <0.001) between nanofiber samples and positive control (100% haemolysis) while non-significant (p value >0.05) between negative control & nanofibers, indicating suitability of fabricated nanofibers in wound healing applications.

4.4.8 *In-vitro* cytocompatibility and cell viability activity

The cell viability and phase contrast image of control, PVA/CH NF and PVA/CH-AgNP-LZNP NF were performed. The results showed good cellular proliferation in nanofibers treatment at 24, 48 and 72 hours (Figure 4.13), which might be due to the 3D matrix structure. The results were in accordance to MTT assay that showed high cell viability by PVA/CH NF and PVA/CH-AgNP-LZNP NF of about 97.02±2.15% & 95.12±2.7% for 24 hr, 93.06±4.15% and 100.49±7.4% for 48 hours and 94.5±2.10% and 94.85±3.04% for 72 hours, respectively (Figure 4.13 B). Further Tukey's multiple comparisons test showed a non-significant difference between test nanofibers and control group at 24, 48 and 72 hours, clearly demonstrating the nanofibers compatibility with HaCaT cell line.

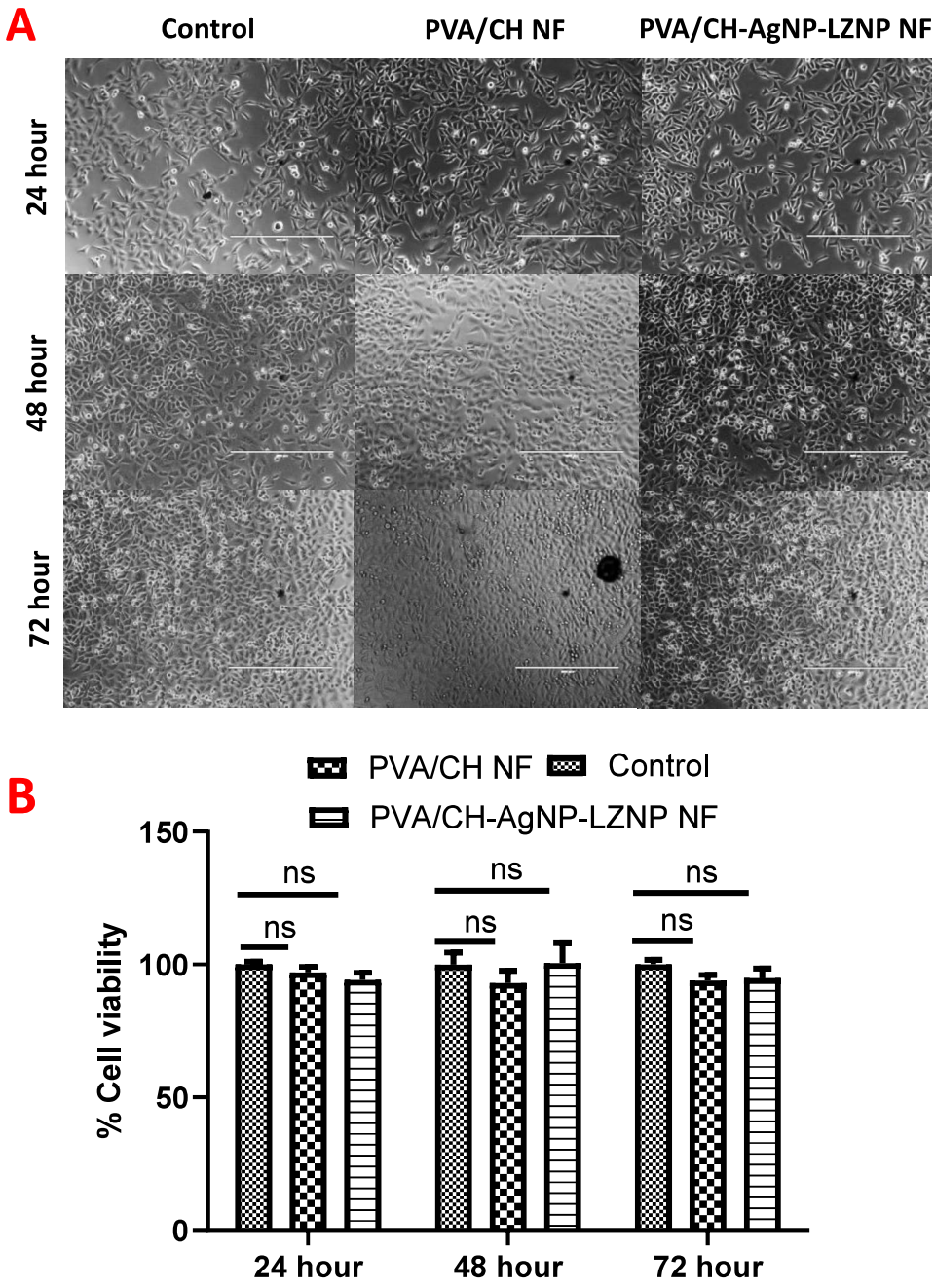

Figure 4.13 (A) Phase contract microscopy images of PVA/CH NF and PVA/CH-AgNP-LZNP NF (White bar represent 400µm); (B) Bar graph showing % cell viability of Control, PVA/CH NF and PVA/CH-AgNP-LZNP NF groups after 24, 48 and 72hr (In graph vertical bars represent standard deviation (n=3) and 'ns' represent non significant difference).

4.4.9 *In-vivo* wound healing activity

The *in-vivo* wound closure study results of PVA/CH NF, PVA/CH-AgNP NF, PVA-CH-LZNP NF, and PVA/CH-AGNP-LZNP NF treatment shown in Figure 4.14. After being infected with *C. albicans,* all groups showed signs of the infections with a wound area of 92.79±2.6% in control group (Untreated), 94.24±2.9% for PVA/CH NF, 94.8±3.48% for PVA/CH-AgNP NF, 96.89±3.772% for PVA/CH-LZNP NF and 96.2±3.13% for PVA/CH-AgNP-LZNP NF group at day 4 (**Figure 4.14**).

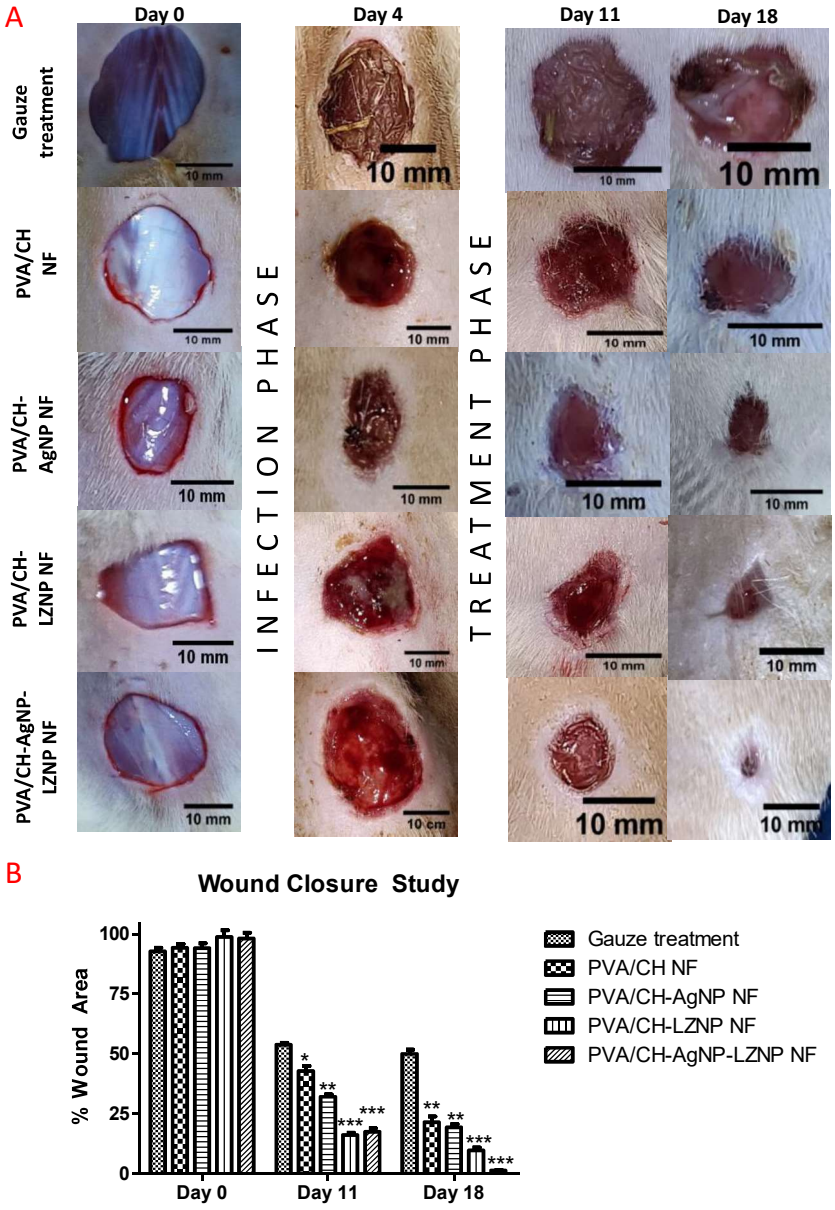

Figure 4.14 Wound image of *In-vivo* wound closure study showing wounds healing in PVA/CH NF, PVA/CH-AgNP NF, PVA-CH-LZNP NF, and PVA/CH-AGNP-LZNP NF treatment groups at Day 0, 4, 11 and 18; (B) Bar graph showing % wound area over time graph (In graph vertical bars represent standard deviation (n=3), * represent p value < 0.05, ** represent p value < 0.01 and *** represent p value < 0.001).

On 11th day, untreated group displayed poorest wound healing (wound area of over 50%) compared to other. On day 18, PVA/CH NF treated group higher wound closure (wound area of 21.520±3.986%) with limited signs of infection than untreated group. This could be due to chitosan-based NF that prevented bacterial invasion. The PVA/CH-LZNP NF and PVA/CH-AgNP NF did not showed any signs of infection and had faster wound closure (wound area of 9.7±2.11% and 19.32±2.4%, respectively) at Day 18. The wound area was also significantly different (p value <0.01) for PVA/CH-AgNP NF and PVA/CH-LZNP NF at day 11 and 18. Finally, PVA/CH-AgNP-LZNP NF demonstrated highest wound healing than other groups (<p 0.001) at day11 (wound area of 17.45±2.51% for) and day 18 (wound area of 1.30±0.32%). The results indicated the effectiveness of PVA/CH-AGNP-LZNP NF in treating *C. albicans* infected wound.

4.4.10 Histological study

The histological examination of nanofiber treated wound closure was conducted successfully. (**Figure 4.15**). The untreated group showed a clear sign of fungal infection in its histological examination on day 11 and 18 of the study. The PVA/CH NF groups also showed signs of inflammatory cells as response to infected wound site along with minor to moderate re-epithelialisation. The PVA/CH-AgNP NF and PVA/CH-LZNP NF group showed moderate re-epithelization at day 11 and minor signs of granulation and collagen formation on day 18. PVA/CH-AgNP-LZNP NF had excellent granulation sign on day 18 revealing better wound healing compared to other groups.

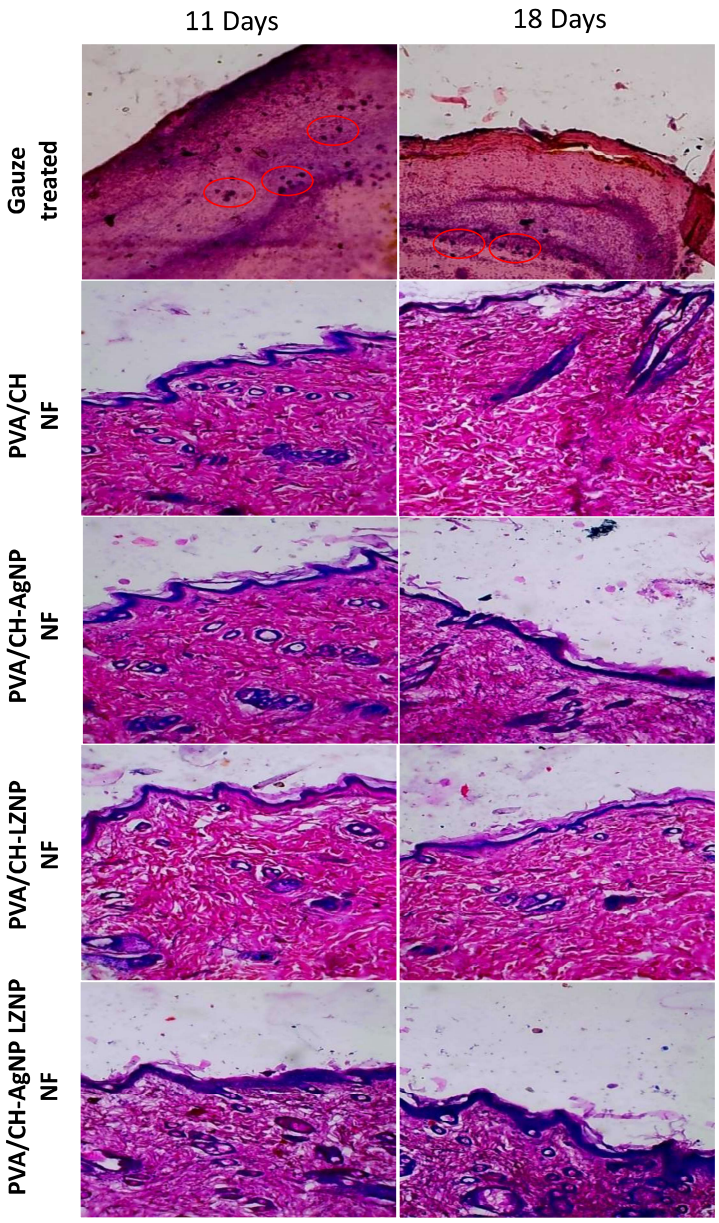

Figure 4.15 Histological study result of different treatment groups at Day 11 and 18 of study

4.4.11 Laser doppler study

Laser doppler is a well-known method for blood flow estimation in skin or at wound site [251–254]. The laser doppler results (**Figure 4.16**) showed low blood flow in untreated group (15.33±3.513) at wound site on Day 11, that might be due to microbial biofilm formation that retarded the healing process. The PVA/CH NF group displayed a

significantly higher blood flow (20.667±1.528) than untreated group probably due to stealth layer provided by nanofiber

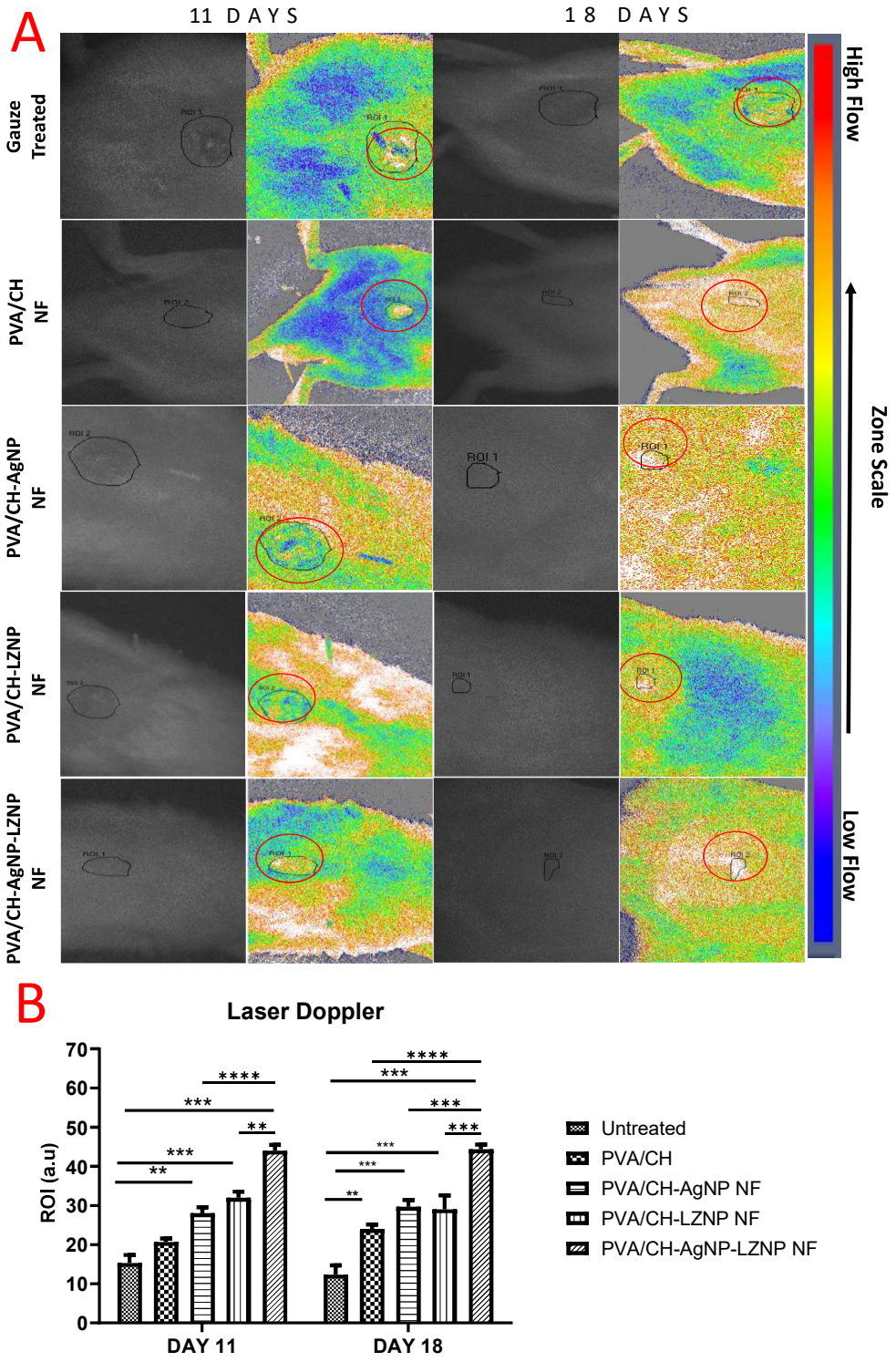

Figure 4.16 (A) Laser doppler study of different treatment groups showing blood flow around wound area; (B) Bar graph of ROI values obtained from laser doppler in different treatment groups on day 11 & 18 (In graph vertical bars represent standard deviation (n=3), ** represent p value < 0.01, *** represent p value < 0.001, and **** represent p value < 0.0001).

as well as antibacterial role of chitosan that avoided the invasion of microbes at wound site. The PVA/CH-AgNP NF and PVA/CH-LZNP NF groups significantly improved the blood flow to a higher extent (28.1 ±2.46 and 32±3.15, respectively), attributed to antimicrobial and antifungal activity of AgNP and LZNP. Whereas, PVA/CH-AgNP-LZNP NF group exhibited highest blood flow of 44.4±1.4 and 45.72±2.05 on days 11 and 18 due to combined effect of AgNP and LZNP. And blood flow was significantly (p value <0.01) improved compared to other groups.

4.5 Discussion & conclusions

The work involved design of silver nanoparticles and luliconazole nanoparticles, subsequently loaded in nanofibers to give anti-infective wound dressing material for treatment of infected wound. Silver nanoparticles were prepared using glutathione as reducer and the synthesis was confirmed by a pale yellow-green colour observed on successful synthesis of AgNP [238]. TEM and SEM results confirmed the AgNP in range of 5-20nm [255]. LZNP formulated exhibited a size of sub-200 nm (Figure 1B) with a distinctive spherical morphology & homogeneous particle distribution. The TEM further confirmed the structural characteristics of AgNP and LZNP loaded nanofibers, showing an interconnected nanofibers with AgNP dispersed homogenously in the core of nanofibers [256], while LZNP as bulb on surface. SEM and AFM results of PVA/CH-LZNP & PVA/CH-AgNP-LZNP NF were also in accordance with TEM, showing LZNP bulge over nanofiber surface. The results provided valuable insights on nanoparticles co-loaded within the nanofibrous structures as carrier [122,257]. Spectroscopic methods also confirmed the proper encapsulation of nanoparticles in nanofibers with high biocompatibility between

drug and polymer [258] [259] [260]. The surface characteristic like pH and hydrophilicity of fabricated nanofibers fall within desired range (i.e., 5.8–6.8 pH of healthy skin and high wetting potential with low contact angle of 55.66±3.5^{o}), suggesting the acceptability of fabricated nanofibers for application at target site [250,261,262]. The fabricated nanofibers was also cytocompatibility against HaCaT cells, and thus will not exert any adverse effect when applied at wound site [232,263,264]. The entrapment efficiency also confirmed the high capacity of fabricated nanofibers in co-loading nanoparticles for desired application [265]. The nanofiber was capable of providing controlled drug release following Korsmeyer-Peppas model. The release mechanism was attributed to erosion or swelling-controlled Fickian diffusion [266]. Similarly, release of silver ions followed a zero-order kinetics, providing drug release for >96 hours. The real-time drug release from fabricated nanofibers was also confirmed using *in-vivo* imaging study that provided favourable evidence of controlled drug release at wound site from the nanofibers. The antifungal and antibiofilm study were also conducted against fungal strains prone to infect wound site and thus forming biofilm, delaying healing process and further severing the wound. Fabricated nanofiber exhibited strong antifungal activity against all five strains of candida species and also strong antibiofilm activity against *C. albicans* & *C. tropicalis*. This could be due to silver nanoparticles and luliconazole nanoparticles loaded in nanofibers as silver and luliconazole have potent antifungal activity against the candida species [267,268] [269]. The mechanism of action is dependent on silver ions role in disrupting the integrity of fungi cell wall and alteration of signal transduction [270] while luliconazole role in inhibiting lanosterol demethylase to disrupt cell membrane and thus cell death [197,271]. Therefore, fabricated nanofibers co-loaded with silver nanoparticles and luliconazole nanoparticles resulted in a dressing material with potent antifungal activity for application at infected wound.

The capability of fabricated nanofibers in curing infected wound was further confirmed by *in vivo* wound closure study. The untreated group infected with fungal strain had poor healing, compromised wound closure and low blood flow at wound site [15]. This highlighted the adverse impact of infection in wound healing, and thus necessitated for demand of anti-infective treatments. Fabricated nanofibers found to have role in allowing gaseous exchange, maintaining moist environ, provided stealth to microbial invasion, supported cell proliferation, and improved blood flow at wound site, all together fasten the wound healing [272]. The nanofibers significantly accelerated the healing process of infected wounds compared to untreated group due to their inherent antifungal activity owing to loaded nanoparticles (AgNP and LZNP) [269].

In conclusion, effective diabetic wound management requires a combination of specialised wound care techniques, addressing underlying factors, and involving a multidisciplinary effort. Fabricated nanofibrous wound dressing material equipped with antifungal agents can offers potent therapeutic activity against fungal strains that infects wounds and delay the healing. Fabricated nanofibers could emerge as a novel method for accelerating the healing process and shortening the wound closure period of infected wounds, thereby improving the quality of life and patience care.